Supporting Online Material For:

Polydispersity-Driven Block Copolymer Amphiphile Self-Assembly into Football-Shaped Micelles

Andrew L. Schmitt, Milton H. Repollet-Pedrosa, Mahesh K. Mahanthappa*

Department of Chemistry, University of Wisconsin-Madison, 1101 University Avenue, Madison, WI 53706 (USA)

Contents

OBO synthesis

OBO triblock copolymers with polydisperse middle B blocks were synthesized using tandem chain transfer ring-opening metathesis polymerization (ROMP-CT) and anionic ring-opening polymerization (AROP). ROMP of 1,5,9-dodecatriene with the difunctional chain transfer agent *trans*-1,6-bis(trifluoroacetoxy)-3-hexene yields a α,ω-dihydroxy-poly(1,4-butadiene) macroinitiator, which was then chain-extended by living anionic polymerization of ethylene oxide initiated by potassium naphthalenide. Monodisperse OBO triblock copolymers (control samples) were synthesized bya two step procedure. In the first step, anionic polymerization of 1,3-butadiene initiated with 3-(triisopropylsiloxy)-1-propyl lithium (TIPSOPrLi), followed by living chain end capping with ethylene xodei and fluoride-deprotection of the sloxy endgroup yielded a monodisperse α,ω-dihydroxy-poly(1,4-butadiene). This telechelic was then used a macroinitiator for the living anionic ring-opening polymerization of ethylene oxide. These materials have been fully characterized using ^{1}H NMR, SEC, and polymer degradation analyses of the end blocks, to independent analyze each homopolymer segment of the copolymers as reported in Table S1.[1]

OBO Molecular Characterization

Table S1. Molecular and Melt-phase Characterization of OBO Triblock Copolymers

sample	$M_{n,B}$[a]	PDI B[a]	$M_{n,O}$[b]	PDI O[c]	$M_{n,total}$[b]	PDI_{OBO}[d]	f_B[e]	N_{total}[f]	D_{exp} (nm)[g]	$(\chi_{OB}N)$[i]	Melt-Phase Morphology
OBO-w58	9.3	1.74	13.0	1.25	22.3	1.37	0.48	331	43.6	43	cylinders
OBO-w48	9.3	1.74	6.7	1.20	16.0	1.46	0.64	247	33.2	32	lamellae
OBO-w24	9.3	1.74	2.9	1.22	12.2	1.68	0.80	197	27.0[h]	26	cyl. + lam.
OBO-w18	11.2	1.75	2.4	n.d.	13.6	1.91	0.86	223	28.6	29	dis. cyl.
mOBO-w68	10.0	1.05	21.7	n.d.	31.7	1.08	0.37	457	22.3	59	lamellae
mOBO-w51	10.0	1.05	10.4	n.d.	20.4	1.07	0.55	308	17.2	40	lamellae

[a] Determined by SEC using a Mark-Houwink corrected polystyrene calibration curve. [b] Calculated from $M_{n,B}$ from SEC and quantitative ^{1}H NMR of the triblock copolymer. [c] Determined directly by absolute molecular weight characterization by SEC of the O homopolymer products of metathesis degradation (see text for details). [d] PDI = M_w/M_n determined using SEC against a conventional polystyrene standard calibration curve. [e] f_B = volume fraction of poly(1,4-butadiene) determined by quantitative ^{1}H NMR composition analyses and the homopolymer melt densities at 140 °C.[2] [f] Volume normalized degree of polymerization calculated using a 118 Å^3 monomer reference volume. [g] calculated based on the principal reflection q^* from synchrotron SAXS. [h] measured lamellar *D*-spacing; the *D*-spacing for the cylinders morphology is 24.0 nm. [i] Calculated at 170° C based on $\chi_{OB} = 0.13$ at 170 °C from OB1-6 ($N_{vol,\ tot} = 82$, $f_B = 0.51$,[3] and the mean field result for diblocks, $(\chi N)_{ODT} = 10.495$).

OBO Aqueous Dispersion Preparation

1 wt% OBO aqueous dispersions were made by inducing micellization from a selective solvent. De-ionized water was added to a rapidly stirred 10 wt% polymer solution in THF to a total volume such that the final polymer concentration was 1 wt%. The solutions were vigorously stirred for 1 day. These solutions were then dialyzed against deionized water using Spectra/Por dialysis membranes (M_w cutoff of 6 kDa) for 7 days, during which the deionized water reservoir was changed daily.

Dynamic light scattering (DLS).

DLS was performed on a Beckman Coulter N5 Submicron Particle Size Analyzer equipped with an 80 Multi-TAU channel digital correlator and He-Ne laser with a wavelength of 632.8 nm. Samples were filtered (0.45 μm pore size) into a dust-free glass cuvet. Multi-angle light scattering experiments were conducted at 30°, 60°, 90°, 120° and 150°. The second-order auto-correlation functions from each scattering vector, q, were fit using either a single exponential with a cumulant expansion to capture the particle size polydispersity index (PI) or a double exponential decay for multimodal scatterer populations (Eq. S1 and S2, respectively) to determine the relaxation decay/s, Γ. The diffusion coefficients, D_t, and thus the radius of hydration, R_H, are found from fitting Γ vs. q^2 plots (Eq. S3) and applying the Einstein Stokes relation for the diffusion of hard spheres (Eq. S4).

$$g^{(2)}(\tau) - 1 = \beta\, e^{-2\Gamma\tau}\left(1 + \frac{\mu_2\,\tau^2}{2!}\right)^2 \qquad \text{Eq. S1}$$

$$g^{(2)}(\tau) - 1 = (A_1 e^{-\Gamma_1\tau} + A_2 e^{-\Gamma_2\tau})^2 \qquad \text{Eq. S2}$$

$$\Gamma = D_t\, q^2 \qquad \text{Eq. S3}$$

$$R_H = \frac{k_B\, T}{6\pi\,\eta\, D_t} \qquad \text{Eq. S4}$$

Relaxation decays for polydisperse samples with high hydrophilic content, OBO-w42 and OBO-w58 (Figure S1 (a)) were best described using a single exponential decay with a cumulant expansion to determine the polydispersity index (PI) of micellar sizes (a PI = 0 indicates a completely monodisperse ensemble). Polydisperse samples with low hydrophilic content, OBO-w18 and OBO-w24 (Figure S1 (b)) were fit using a double exponential decay function, as single exponential decay fits with cumulant expansion resulted in poor fits of the relaxation decays. Monodisperse OBO-w51 and OBO-w68 were also best fit using single exponential decay with cumulant expansion (Figure S1 (c)).

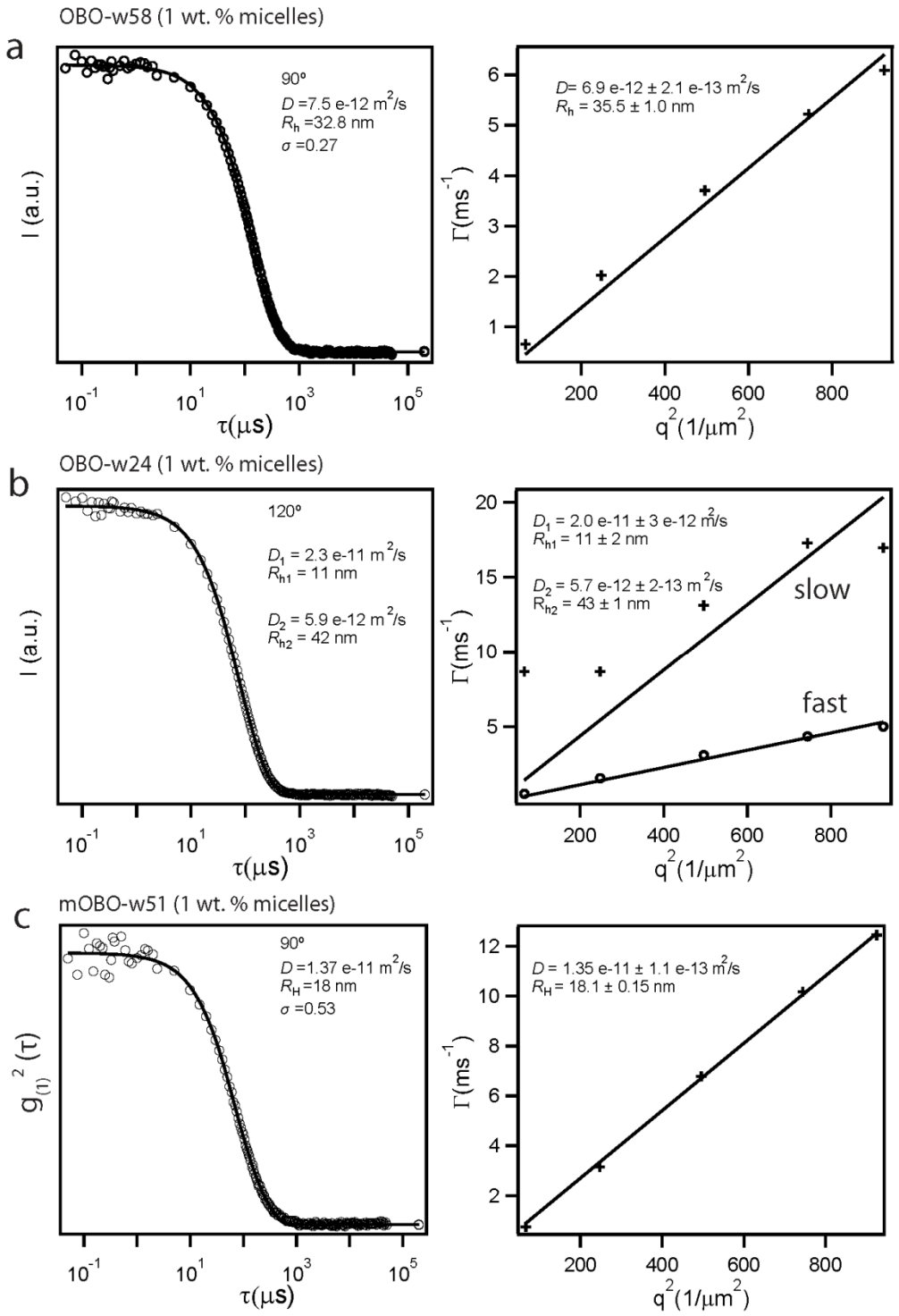

Figure S1. Dynamic light scattering of polydisperse OBO-w58 (a), OBO-w24 (b), and monodisperse mOBO-w51. Panels on the left show fits of the second-order autocorrelation function using single-exponential decay functions with a cumulant expansion for (a) and (c), and a double-exponential decay in (b). Double exponential decay gives information about slow (large) and fast (small) scattering populations in this apparently bimodal sample.

Synchrotron Small Angle X-ray Scattering

Synchrotron SAXS was performed on the DuPont-Northwestern-Dow Collaborative Access Team 5-ID-D beamline (Sector 5) at the Advanced Photon Source (APS) at Argonne National Lab (Argonne, IL). 5 wt% micellar solutions were loaded into quartz capillaries and exposed to x-rays with an incident beam energy of 16 keV (λ = 0.7293 Å) and a 3.068 m sample-to-detector distance for 5 s. Two-dimensional SAXS patterns were recorded at 1024 × 1024 pixel resolution on a MAR-CCD detector (133 mm diameter active circular area) and calibrated against silver behenate. Isotropic 2D SAXS patterns were azimuthally integrated to obtain one-dimensional intensity *versus* scattering wavevector (q) plots. These plots were background corrected using an H_2O blank and fitted to various form factor scattering models using IRENA software developed by Jan Ilavsky at APS.[4] X-ray contrast was calculated for the core (poly(1,4-butadiene)), the shell (poly(ethylene oxide)), and the solvent (water) based on electron density. Simple sphere models fail to describe micelle x-ray scattering, even for monodisperse samples. The corona block PEO is either collapsing near the core and/or increasing the electron contrast of the water in the corona. Core-shell models with shell electron densities larger than water more adequately fit the data (OBO monodisperse control sample mOBO-w68 shown as example, Figure S2). In each least-squares fitting the corona/shell width ($R_{particle} - R_{core}$) was found to be 8-9 nm; whereas the full corona width from geometrical standpoint must be much larger. Fits of OBO-w42 for rod-like core-shell model that approximates the anisotropy of a prolate spheroid are better than those provided by core-shell sphere models. SAXS fits for these low contrast samples are not particularly helpful and provide limited information in the limit of low (< 2-3) anisotropy.

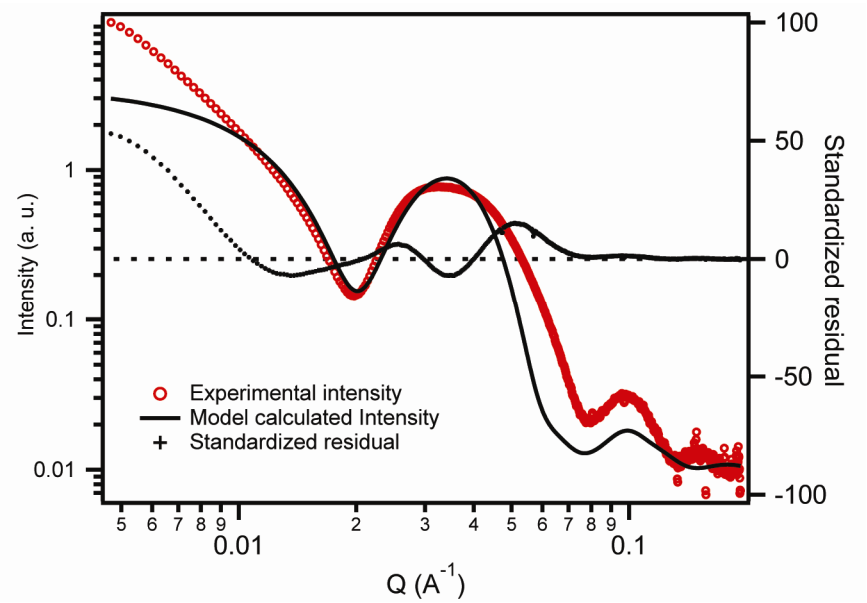

Figure S2. Synchrotron SAXS from a 5 wt% micellar dispersion of mOBO-w68 fit using core-shell sphere model with a Gaussian distribution of sphere sizes. Best fit parameters are R_{core} (12.7 nm), $R_{particle}$ - R_{core} (8.5 nm), and the width of the distribution (2.0 nm).

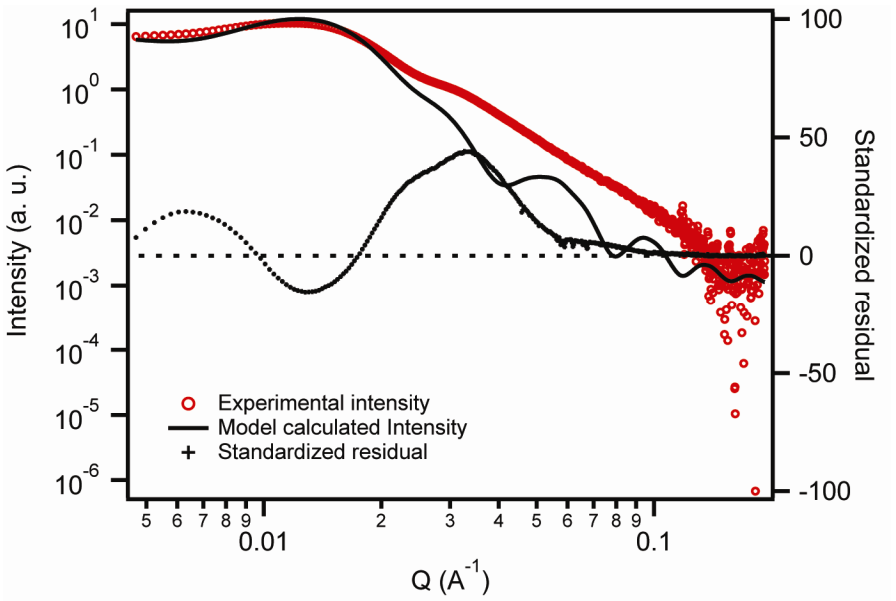

Figure S3. Synchrotron SAXS from a 5 wt% micellar dispersion of OBO-w42 fit using core-shell sphere model with a Gaussian distribution of sphere sizes. Best fit parameters are R_{core} (34.5 nm), $R_{particle}$ - R_{core} (8.0 nm), and the width of the distribution (8.0 nm).

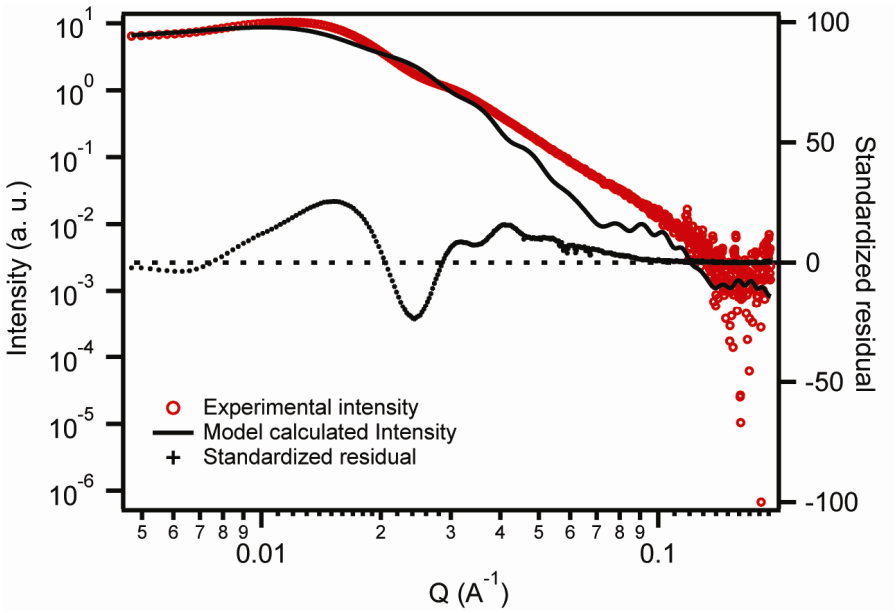

Figure S4. 5 wt% OBO-w42 fit using rod-like core shell model. Synchrotron SAXS from a 5 wt% micellar dispersion of OBO-w42 fit using a rod-like core-shell model with a log normal distribution of sphere sizes. Best fit parameters are R_{core} (20.0 nm), standard deviation (0.5), $R_{particle}$ - R_{core} (9.0 nm), and rod (long) axis (46.0 nm). The resulting anisotropy is 1.2.

Differential Scanning Calorimetry

DSC analyses were performed using a TA Instruments Q100 modulated differential scanning calorimeter under nitrogen atmosphere. Pure OBO-w42 polymer and a 1 wt% OBO-w42 micellar solution were hermetically sealed in aluminum pans. The pure polymer was cooled to -30 °C and heated to 220 °C using a heating ramp rate of 10 °C/min. The micelle solution was cooled to 5 °C and heated at 5 °C/min to 80 °C (Figure S5).

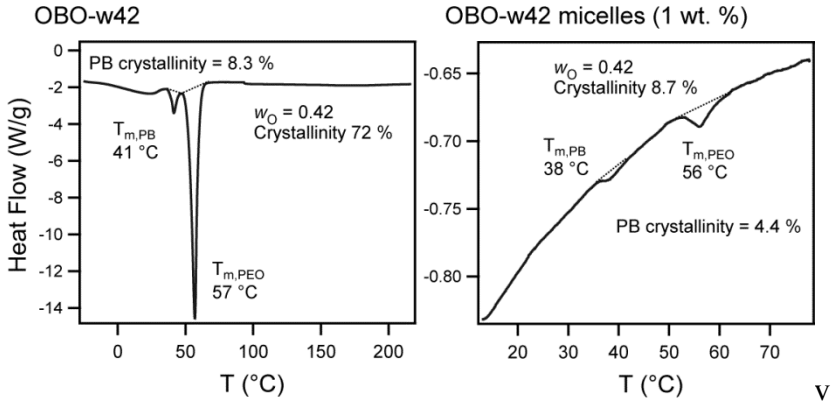

Figure S5. Dynamic scanning calorimetry for pure OBO-w42 and a 1 wt% aqueous dispersion of OBO-w48 in water show that OBO-w42 exhibits 72 wt% O block crystallinity and 8.3 wt% B block crystallinity. The aqueous dispersion has exhibits residual O crystallinity likely due to increased O segment density near the micellar surface that protects the PB from unfavorable contacts with water. B block crystallinity in the micelles decreases to 4.4 wt%, the melting point of this block is slightly depressed in a manner consistent with reduced crystal sizes due to nanoconfinement.

The crystallinity of OBO-w42 and the corresponding micellar dispersion were studied using dynamic scanning calorimetry (DSC). Thermal analysis for the pure triblock reveals melting endotherms upon heating at $T_{m,B}$ = 41 °C and $T_{m,O}$ = 57 °C. Weight percent crystallinity, χ_c, for PEO and PB components was calculated from w_O and the theoretical heat of fusion ΔH_{th} for perfectly crystalline PEO and PB (203 J/g[5] and 85.2 J/g,[6] respectively) using:

$$\chi_{c,O} = \frac{\Delta H_{exp,O}}{\Delta H_{th,O} \times w_O} \qquad \text{Eq. S5}$$

$$\chi_{c,B} = \frac{\Delta H_{exp,B}}{\Delta H_{th,B} \times (1 - w_O)} \qquad \text{Eq. S6}$$

The high *trans* content in the PB middle block gives PB chains that are 8.3 % crystalline below $T_{m,PB}$ = 41 °C in neat polymer. In a 1 wt% solution of OBO-64 micelles, the crystallinity falls to 4.4 % with a decreased $T_{m,PB}$ = 38 °C. Nanoscale confinement and enhanced surface effects are known to suppress

melting points and effect crystallinity and crystalline habits.[7] We note that the crystallinity of the corona PEO blocks is not completely inhibited in the aqueous dispersion. PEO crystallinity drops from 72 %, a typical value for bulk PEO, to 8.7 %. Neutron studies have shown that segmental PEO density is enriched near the core prior to extension out into solution.[8] This observed crystallinity may be due to O segment crystallization near the hydrophilic/hydrophobic interface that shields the micellar core from unfavorable interactions with water.

Cryogenic Transmission Electron Microscopy (CryoTEM).

Vitrified CryoTEM specimens were prepared by placing a 5 μL droplet of the 1% wt. micellar solution on a lacy carbon-coated copper grid (Ted Pella, Inc.) in the Vitrobot (Ted Pella, Inc.), a controlled environment vitrification system, using -2 mm blotting offset, a 1 s blot time, and a 15 s drain time for sample equilibration. Following the drain time, each sample as plunged in liquid ethane (-80 ºC) and transferred under liquid nitrogen to a Gatan 626 DH or a Fischione cryo-transfer specimen holder. TEM imaging was performed at -178 ºC using either a FEI Tecnai G2 F30 TEM operating at 300 kV or a LEO 912 EFTEM operating at 120 kV. Characterization was carried out at the Institute of Technology Characterization Facility at the University of Minnesota and the NSF-NSEC characterization facilities in the Materials Science Center at the UW-Madison.

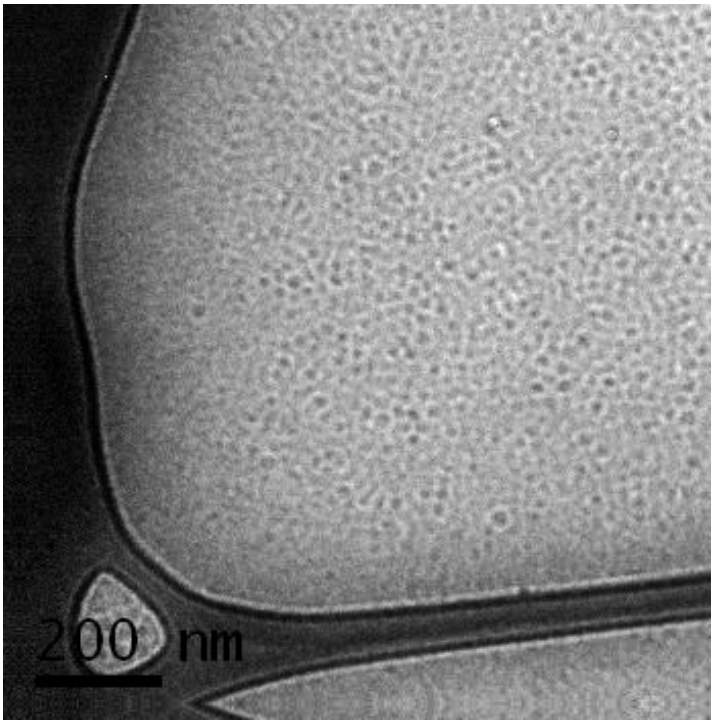

Figure S6. CryoTEM of monodisperse spheres of mOBO-w51.

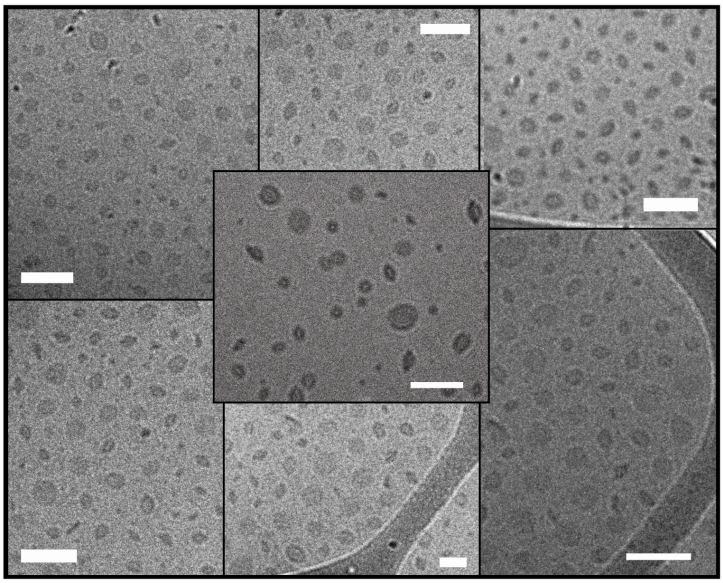

Figure S7. Collage of prolate spheroid morphology adopted by polydisperse OBO surfactants. All scale bars are 100 nm

Analysis of Molecular Weight Distributions

Using the independent assessment of M_n and M_w/M_w (PDI) for each block in our triblock copolymer samples (Table S1), we can reconstruct the unique chain-length distribution function $\rho_{OBO}(N)$ using a Schulz-Zimm distribution (Eq. S4), where N is the volume degree of polymerization of a given chain, $N_{v,tot}$ is the average volume degree of polymerization of the sample, Γ is the gamma function, and k is a parameter describing the breadth of the distribution as given in Eq. S8.

$$\rho_{OBO}(N) = \frac{k^k N^{k-1} e^{-\left(\frac{kN}{N_{v,tot}}\right)}}{\Gamma(k) {N_{v,tot}}^k} \quad \text{Eq. S7}$$

$$k = \frac{1}{PDI-1} \quad \text{Eq. S8}$$

The resulting distributions are weighted by the volume degree of polymerization to yield the volume fraction as a function of N (panel (d) in manuscript Figures 1 and 2).

The approximate critical N_v for each solution morphology was determined graphically based on a previously determined model OB diblock copolymer phase portrait for 1 wt% solutions.[9] The order parameters for the phase diagram are the poly(1,4-butadiene) core volume degree of polymerization, N_{PB}, and the weight fraction of the hydrophilic block, w_O. Compositional polydispersity in these samples implies that each chain has roughly the same length O endblocks and this assumption is used to determine the dependence of N_{PB} on w_O for each sample (Figure S8, OBO-w42 shown). These graphs are then overlaid on the OB diblock phase portrait with identical axis ranges (Figure S9) to determine

the approximate critical values of N_{PB} and hence $N_v = N_{PB} + N_{PEO}$ that are plotted in manuscript Figures 1 (d) and 2 (d). A table containing these values for all polydisperse samples is provided (Table S2).

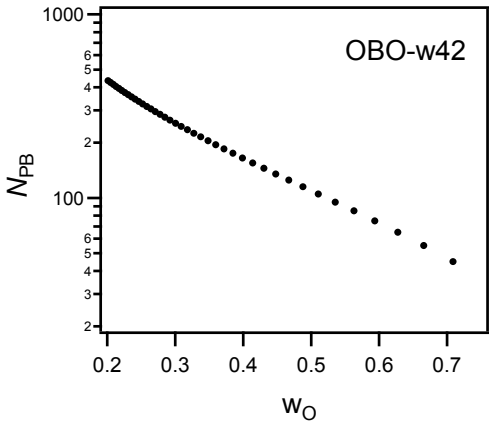

Figure S8. Dependence of N_{PB} on w_O across the inter range of possible w_Os for OBO-w42.

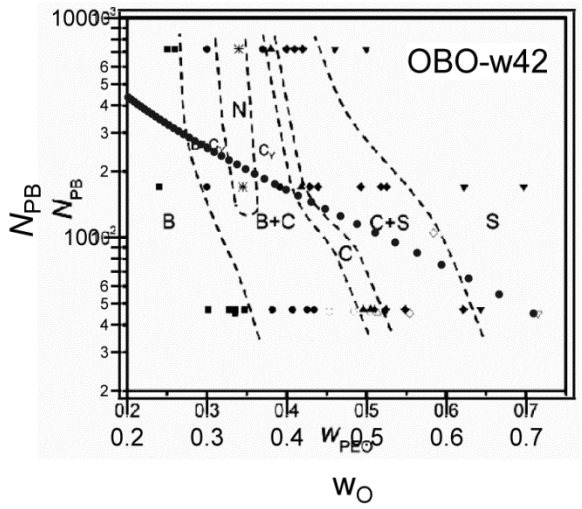

Figure S9. Overlay of the model OB diblock copolymer micellar phase behavior with the N_{PB} dependence on w_O for OBO-w48 on identical axis scales. Critical points are determined from where the dots intersect the approximate transition lines (black dashes). The network phase (N) and y-junctions (C_y) (specific C + B coexistences) have been omitted for clarity.

Table S2. *N*-dependent Phase Boundaries for Micellar Aggregation Polydisperse OBO Samples

	OBO-w18	OBO-w24	OBO-w42	OBO-w58
S at N_v <	64	76	169	335
S+C at N_v <	81	95	213	422
C at N_v <	93	109	243	483
C+B at N_v <	127	150	334	663

Critical values for $N_v = N_{PB,crit} + N_{PEO}$ are shown for each polydisperse sample. The first row holds values of N_v above which spherical micelles (S) are the preferred morphology. The second row indicates values of N_v above which spherical micelles are expected in coexistence with cylinders (C). The third row indicates the N_v above which only cylinders are expected, and the fourth row are N_vs above which cylinders are expected in coexistence with vesicle bilayers (B), but below which only bilayers are expected.

Ellipsoid mean curvature calculation

The general equation of an ellipsoid is given by:

$$\frac{x^2}{a^2}+\frac{y^2}{b^2}+\frac{z^2}{c^2}=1$$

This surface can be parameterized by two coordinates u and v using:

$$x = a\cos u \sin v$$

$$y = b\sin u \sin v$$

$$z = c\cos v$$

$$u(x,y) = \operatorname{atan}\left(\frac{a\,y}{b\,x}\right)$$

$$v(x,y) = \operatorname{asin}\left(\frac{x+y}{a\,\cos\big(u(x,y)\big)+b\,\sin\big(u(x,y)\big)}\right)$$

The mean curvature is given by:[10]

$$H = \frac{a\,b\,c\,[3\,(a^2+b^2)+2\,c^2+(a^2+b^2-2\,c^2)\cos(2\,v)-2(a^2-b^2)\cos(2\,u)\,sin^2v]}{8\,[a^2\,b^2\,cos^2v+c^2\,(b^2\,cos^2u+a^2\,sin^2u)\,sin^2v]^{3/2}}$$

The curvature along the semimajor axis (x) of the average prolate spheroid is calculated in MathCad using a = 18 nm, b = c = 13 nm along the surface where y = 0, $-18 \le x \le 18$.

References

1. Schmitt, A. L.; Mahanthappa, M. K., Polydispersity-Driven Shift in the Lamellar Mesophase Composition Window of OBO Triblock Copolymers. *submitted* **2011**.

2. Fetters, L. J.; Lohse, D. J.; Richter, D.; Witten, T. A.; Zirkel, A., Connection between Polymer Molecular Weight, Density, Chain Dimensions, and Melt Viscoelastic Properties. *Macromolecules* **1994,** 27, (17), 4639-47.

3. Jain, S. Aqueous Mixtures of Block Copolymer Surfactants. Thesis, University of Minnesota, Twin Cities, MN, 2005.

4. Ilavsky, J.; Jemian, P. R., Irena: tool suite for modeling and analysis of small-angle scattering. *J. Appl. Crystallogr.* **2009,** 42, (2), 347-353.

5. Wunderlich, B., *Macromolecular Physics*. Academic Press: New York, 1980; Vol. Vol. 3.

6. *Polymer Data Handbook*. 2nd ed.; Oxford University Press: New York, 2009.

7. Christenson, H. K., Confinement effects on freezing and melting. *J. Phys. Condens. Mat.* **2001,** 13, (11), R95-R133.

8. Won, Y.-Y.; Davis, H. T.; Bates, F. S.; Agamalian, M.; Wignall, G. D., Segment distribution of the micellar brushes of poly(ethylene oxide) via small-angle neutron scattering. *J. Phys. Chem. B* **2000,** 104, (30), 7134-7143.

9. Jain, S.; Bates, F. S., On the Origins of Morphological Complexity in Block Copolymer Surfactants. *Science* **2003,** 300, (5618), 460-464.

10. Weisstein, E. W. Ellipsoid. http://mathworld.wolfram.com/Ellipsoid.html